Probing current-induced magnetic fields in Au|YIG heterostructures with low-energy muon spin spectroscopy

A. Aqeel,[1] I. J. Vera-Marun,[1,2] Z. Salman,[3] T. Prokscha,[3] A. Suter,[3] B. J. van Wees,[1] and T. T. M. Palstra[1,a)]

[1]*Zernike Institute for Advanced Materials, University of Groningen, Nijenborgh 4, 9747 AG Groningen, The Netherlands*

[2]*School of Physics and Astronomy, The University of Manchester, Schuster Building-2.14, Manchester M13 9PL, United Kingdom*

[3]*Laboratory for Muon-Spin Spectroscopy, Paul Scherrer Institute, WLGA/U119, CH-5232 Villigen, Switzerland*

(Received 25 September 2016; accepted 22 January 2017; published online 8 February 2017)

We investigated the depth dependence of current-induced magnetic fields in a bilayer of a normal metal (Au) and a ferrimagnetic insulator (Yttrium Iron Garnet—YIG) by using low energy muon spin spectroscopy (LE-μSR). This allows us to explore how these fields vary from the Au surface down to the buried Au|YIG interface, which is relevant to study physics like the spin-Hall effect. We observed a maximum shift of 0.4 G in the internal field of muons at the surface of Au film which is in close agreement with the value expected for Oersted fields. As muons are implanted closer to the Au|YIG interface, the shift is strongly suppressed, which we attribute to the dipolar fields present at the Au|YIG interface. Combining our measurements with modeling, we show that dipolar fields caused by the finite roughness of the Au|YIG interface consistently explain our observations. Our results, therefore, gauge the limits on the spatial resolution and the sensitivity of LE-μSR to the roughness of the buried magnetic interfaces, a prerequisite for future studies addressing current induced fields caused by the spin-accumulations due to the spin-Hall effect. *Published by AIP Publishing.* [http://dx.doi.org/10.1063/1.4975487]

Recently the exciting field of spintronics has been transformed by the concepts to manipulate the spin transport taking place at the interfaces between magnetic and non-magnetic materials.[1,2] Therefore, it is important to understand the spatial distribution of spin accumulation in different devices. The spin accumulations at these interfaces have been mostly created electrically by the spin-Hall effect (SHE) by sending a charge current through normal metal (NM) with strong spin-orbit coupling[3–5] on top of the magnetic insulators like Yttrium Iron Garnet (YIG). These electrically created spin accumulations are usually detected by an indirect method called spin-Hall magnetoresistance effect in which the resistance of the NM changes with the magnetization of the underlying YIG.[6] In these electrical measurements used to probe SHE, the ever-present background contributions like Oersted fields (the magnetic fields generated by current flowing through a metal) and dipolar fields (the inhomogeneous magnetic fields arising from the roughness of a magnetic surface) cannot be disentangled. Any technique that would aim to estimate these background contributions needs to be spin and magnetic field sensitive along with spatial resolution.

Muon spin spectroscopy is widely used as a magnetic spin microprobe to investigate the superconductivity,[7,8] magnetism[9,10] and many other fields.[11] In addition, low-energy muon spin rotation spectroscopy (LE-μSR) provides an opportunity to tune the energy of the muons (1–30 keV) to perform depth resolved internal field measurements in the range of 1–200 nm.[11–13] Due to the combination of sensitivity[10] and the spatial resolution,[11] LE-μSR has been applied to obtain the depth-resolved profile of the local magnetization in various thin films and heterostructures.[14,15]

All these successful applications of LE-μSR motivate the study of its limits and capabilities in order to gauge the possibility of using such a technique for other sources of current-induced fields, e.g., due to the spin-accumulation by SHE, Oersted fields or magnetization induced via proximity at buried interfaces. To explore this, we considered here a Au|YIG test structure. In this structure, due to the small spin-Hall angle of Au, we expect a negligible contribution from SHE, which allows us to quantify the other current-induced contributions, such as ever-present Oersted fields and dipolar fields due to finite interface roughness. We report here the quantitative study of the depth distribution of magnetic fields in the Au|YIG system with LE-μSR.[16,17]

Fig. 1(a) shows the device configuration used to quantify the current-induced magnetic field distribution at different depths in the Au|YIG heterostructure. The YIG has a thickness of 240 nm grown by liquid phase epitaxy on 0.5 mm-thick (111) Gadolinium Gallium Garnet (GGG) monocrystalline substrate. In any NM|YIG system, there would be two main contributions to a current-induced magnetic field: one would be the spin accumulation due to SHE (see Fig. 1(b)) and other due to Oersted fields (see Fig. 1(c)). Note that for the Au metal (used here), we expect a spin diffusion length of 35 nm (Ref. 18) which would make it compatible with the depth-resolved studies of spin accumulation using LE-μSR. Nevertheless, for the specific case of SHE, the small spin-Hall angle makes the expected signals two orders of magnitude smaller than the Oersted fields, therefore in the current study, we focus on quantifying the latter.

a)E-mail: t.t.m.palstra@rug.nl

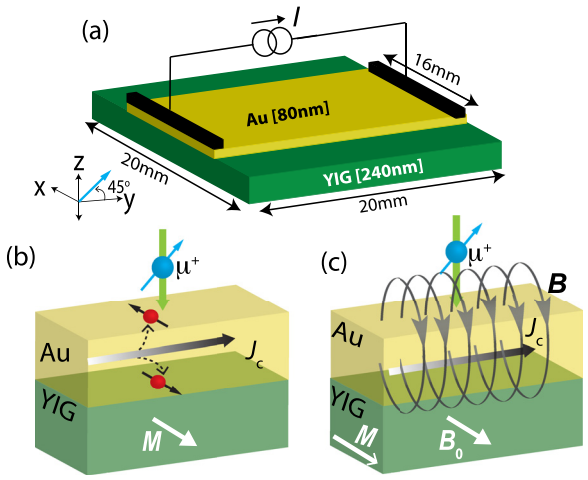

FIG. 1. (a) Device configuration for probing current-induced magnetic fields at Au|YIG interface with muons. (b) Schematic illustration of spatial directions of electrically created spin accumulation created by spin-Hall effect and (c) Oersted magnetic fields $\boldsymbol{B}$ with respect to muon beam μ^+. Here, J_c, $\boldsymbol{M}$, and $\boldsymbol{B}_0$ represent the applied dc-current, magnetization of the YIG film and the applied magnetic field.

All measurements were performed at the LE-μSR spectrometers at the Paul Scherrer Institute, Villigen, Switzerland. The measurements were done at pressure $\leq 10^{-9}$ mbar in a cold finger cryostat. In these measurements, 100% spin polarized positive muons are implanted into the Au|YIG sample, with their spin polarization direction at an angle of 45° in the yz-plane (see Fig. 1). The implanted muons have a short lifetime of 2.2 μs after which they decay by emitting a positron, preferentially in the direction of the muon spin at the time of decay. The reference measurements at different temperatures show no significant temperature dependent spin depolarization of muons. The measurements reported here are done using the transverse field geometry, where the applied magnetic field ($B_0 = 100$ G) is perpendicular to the initial spin direction of the implanted muons (shown in Fig. 1). The decay positrons are detected using appropriately positioned detectors, to the left and right of the sample, relative to the incoming muons. The asymmetry, $A(t)$, the difference of the detected positrons in the left and right detectors normalized by their sum is proportional to the time evolution of the muon spin polarization, which provides information regarding the local magnetic properties at the muon stopping site.

The measurements are performed at different implantation energies and applied currents. By varying the energy of the muons, they can be implanted at different depths in the Au metal. Muons stopping in the YIG depolarize much faster and do not contribute to the measured precession signals. The obtained μSR spectra were analysed using the MUSRFIT software.[19] We find that the collected spectra at all implantation energies and applied currents fit best to Eq. (1)

$$A(t) = A_0 e^{-\lambda t}\cos(\omega t + \phi). \tag{1}$$

Here $\omega = \gamma B$, γ being the muon gyromagnetic ratio, which reflects that the muons experience a Lorentzian field distribution with an average field B and width λ, and ϕ is the angle between the direction of the initial spin polarisation of the muon (at t = 0) and the direction of positron emission. The Larmor frequency ω provides the information about the internal field at the muon site and the damping λ gives information about the inhomogeneity of the internal field at the muon site.

The results of the fit parameters from Eq. (1) are shown in Fig. 2. For the damping λ we do not observe any trend versus current therefore in Fig. 2(a) we show λ only for zero current. Contrary to λ, there is a clear current dependence of the field shift ΔB. This dependence of ΔB is clearly larger at lower energies and gradually decreases until it fully disappears at higher energies ($E \approx 12$ keV), as shown in Fig. 2(b). When muons are implanted closer to the interface, ΔB almost disappears. The internal field at the muon site is also measured at zero current density to rule out other magnetic field-induced effects like proximity effects consistent with the current understanding of the NM|YIG films.[20] A clearer observation of the current dependence of ΔB for different energies is shown in Fig. 2(c): ΔB varies linearly with the applied current closer to the surface of the Au film at $E = 6.4$ keV and almost vanishes closer to the interface at $E = 17.5$ keV.

To interpret the data, we can model the expected field shifts due to current-induced fields as

$$\Delta B_{\lambda'}(E) = \frac{1}{\int_{z=0}^{z=d} \frac{P(E,z)}{\lambda'(z)}dz} \int_{z=0}^{z=d} \frac{P(E,z)}{\lambda'(z)} B(z)dz, \tag{2}$$

where $B(z)$, $P(E, z)$, and $\lambda'(z)$ represent the current-induced Oersted fields, muon stopping profile, and damping due to inhomogeneous fields close to Au|YIG interface. The Oersted fields for a uniform current density J through the Au film can be calculated using $B = -\mu_0 J z' \hat{x}$ for $z' = z - t_{Au}/2$, where t_{Au} and z are the thickness the of Au film and the distance from the surface of Au towards the Au|YIG interface, respectively. We simulated the muon stopping profiles $P(E, z)$ by using the Trim. SP Monte Carlo program,[19] as shown in Fig. 3(a). To get a clear relation between the muon

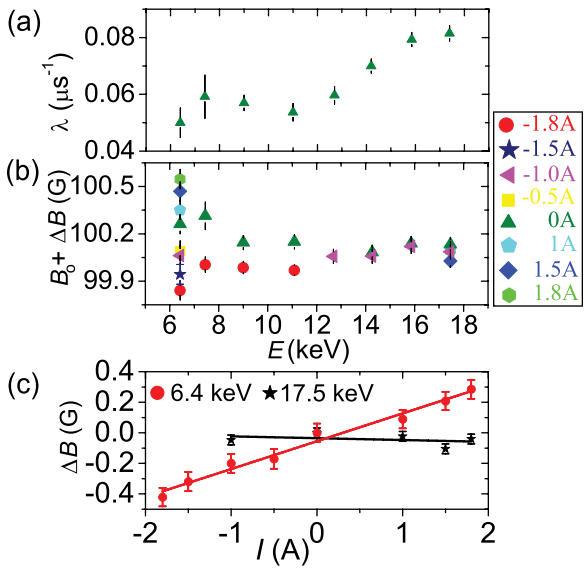

FIG. 2. (a) and (b) shows the observed damping λ and field $B_0 + \Delta B$ as a function of the implantation energy E of muons at different values of applied current (I = −1.8 A to 1.8 A) in the Au|YIG bilayer system, respectively. Here, B_0 represents the applied field. (c) Shift in the internal field ΔB at muon site as a function of the applied current I through the Au film at energies $E = 6.4$ keV, 17.5 keV.

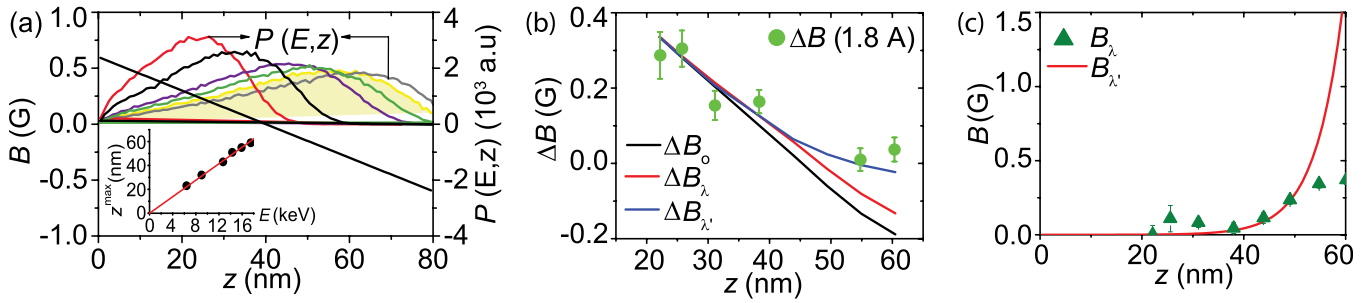

FIG. 3. (a) The current-induced magnetic field as a function of depth z, where z is the distance from the surface of Au towards the interface. $P(E, z)$ shows the probability distribution of the stopping depth of muons as a function of z at different implantation energies E varying from 6 keV to 18 keV. The inset of (a) shows the depth z^{max} of the peak maxima for each probability distribution $P(E, z)$ shown in (a) versus E. It provides a scale ($z^{max} = 3.455 \times E$) to translate from E to depth z for (b) and (c), where $z = z^{max}$. (b) Comparison of the observed field shifts ΔB with the calculated shifts ΔB_o, ΔB_λ, and $\Delta B_{\lambda'}$ at different implantation energies of muons. Here, ΔB_o, ΔB_λ, and $\Delta B_{\lambda'}$ represent the field shifts including, only the muon depth distribution profiles, the effect of observed damping λ shown in Fig. 2(a), and the effect of estimated damping λ' due to the dipolar fields, respectively. (c) Comparison between the field B_λ calculated by considering the observed λ and the dipolar field $B_{\lambda'}$ (using Eq. (3)) as a function of distance z.

implantation energy and the depth, we relate each energy to the peak position z^{max} of the muon distribution profile, as shown in the inset of Fig. 3(a).

The presence of any additional inhomogeneous field at the muon site can lead to the precession of muon spins at different frequencies and gives rise to damping of the muon signal which we include in Eq. (2) by a parameter $\lambda'(z)$. This damping which we include as $\lambda'(z)$ can prevent us from observing the expected field shift ΔB. The observed damping $\lambda(E)$ (shown in Fig. 2(a)) increases by a factor of two closer to the Au|YIG interface, also suggests the presence of these inhomogeneous fields $B_{\lambda'}$ closer to the interface. This inhomogeneity in the field $B_{\lambda'}$ is given by the expression $B_{\lambda'} = \lambda'(z)/2\pi\gamma$.

There are several mechanisms that can cause these inhomogeneous magnetic fields (therefore $\lambda'(z)$) close to the interface which can influence the expected magnetic field shifts including nuclear hyperfine fields,[21–23] the dipolar fields from magnetic domains[24] or the interface roughness.[25,26] The formers are not relevant here, as the nuclear hyperfine fields are too small in Au, typically 0.02 μs^{-1}. We remark that the magnetic domains can be formed by anisotropy but for these films, the anisotropy is not relevant and the thickness of YIG film is still small enough to neglect also the interfacial anisotropy, recently reported in thicker YIG films.[27] Moreover, the coercivity of the YIG film is around 2 G, therefore in these experiments, the film is fully saturated and we can ignore the effect of magnetic domain boundaries. However, the inhomogeneous magnetic fields arising from finite interface roughness can dramatically influence the dynamics of expected magnetic fields at the magnetic interface of multilayer systems.[26] The magnitude of these inhomogeneous dipolar fields scales with the roughness amplitude h and decays with distance z from the interface on a length scale of the lateral roughness η.[26,28] Fig. 4(c) shows the sketch of the dipolar fields near the Au|YIG interface with a finite roughness. The dipolar fields[26] can be estimated as follows:

$$B_{\lambda'}(z) = \mu_0 M_s \frac{h}{2} \sum_{n=1}^{\infty} q_n \frac{\sin\left(\frac{1}{4} q_n \eta\right)}{\frac{1}{4} \eta q_n} \frac{\sin\left(\frac{1}{2} q_n h\right)}{\frac{1}{2} q_n h} \exp(-q_n z). \quad (3)$$

Here $q_n = \frac{2\pi n}{\eta}$ and M_s is the saturation magnetization of YIG. For this model of the sinusoidal interface profile, lateral period $\eta = 20$ nm and roughness amplitude $h = 1$ nm are estimated from the atomic force microscope image of the YIG surface shown in Figs. 4(a) and 4(b). Fig. 3(c) shows the dipolar fields $B_{\lambda'}$ estimated by Eq. (3).

To find the effect of these dipolar fields on the observed field shifts ΔB, we calculated damping λ' associated with the dipolar fields $B_{\lambda'}$ and used in Eq. (2). Fig. 3(b) shows a good agreement between the field shifts $\Delta B_{\lambda'}$ estimated by including dipolar fields and the measured field shifts ΔB, both vanishing closer to the Au|YIG interface. Therefore, we achieved a consistent picture by taking into account the damping λ' due to the dipolar fields resulting from the finite surface roughness.

To check whether the assumption of presence of the inhomogeneous fields $\Delta B_{\lambda'}$ close to the interface is correct, we can estimate these fields by using the observed damping $\lambda(E)$ (Fig. 2(a)). The estimated B_λ is around 0.3 G, which is in the same order as the expected current-induced fields at the interface (cf. Figs. 2(c)–2(c)). However, these B_λ fields are much smaller than the inhomogeneous fields $B_{\lambda'}$ estimated for the dipolar fields at the interface, which can be

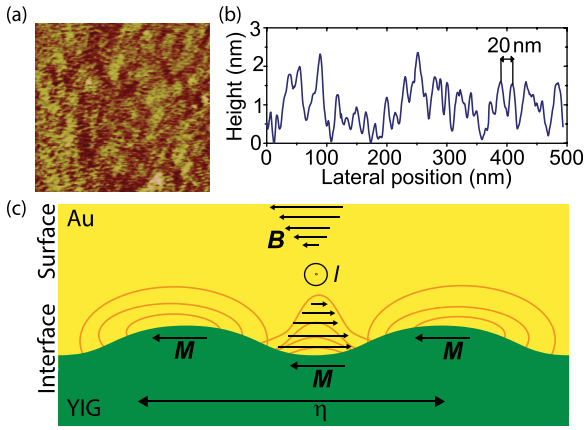

FIG. 4. (a) Atomic force microscope image (500×500 nm^2) and (b) a representative cross-sectional height profile of the YIG surface, prior to the Au metal deposition. (c) Illustration of inhomogeneous dipolar fields near the Au|YIG interface with a finite roughness, sketched for a sinusoidal interface profile with a lateral period η. Here **M** and **B** represent the magnetization of YIG and the current-induced field, respectively.

understood from the fact that B_λ are also convoluted from the muon profile $P(E, z)$, in reality, the dipolar fields can be much larger than these estimated values. Fig. 3(b) shows that the estimated inhomogeneous fields ΔB_λ by using $\lambda(E)$ result in preferential reduction of the shift around 30% close to the interface. To further confirm if the assumption of the inhomogeneous fields $B_{\lambda'}$ at the interface is correct, we can calculate the field shifts without the damping λ' by considering it to be depth independent (i.e., $\lambda'(z) = 1$). Fig. 3(b) shows that the field shifts (ΔB_o) without considering the effect of damping is around 0.2 G at the interface, much larger than the value around 0 G observed close to the interface. Therefore, it confirms that the assumption of dipolar fields at the interface is in good agreement with experimental observations, as shown in Fig. 3(b).

In conclusion, we have established that LE-μSR can indeed work for resolving the background signals present due to interface roughness and Oersted fields which are a universal feature in experiments done to probe SHE, with proper magnitude, distance dependence, and sign. In the current measurements, we obtained a field resolution below 0.1 G. We have to gauge the viability of the SHE by making sure that the induced spin-accumulations create the magnetic field of this order which now would depend on the specific parameters of the material. Moreover, the depth variation in the local magnetic field from SHE is on the scale of 10 nm which is compatible to the resolution of LE-μSR, confirming the suitability of the technique to these measurements. Hence, our results establish a point of reference and a guide for future experiments aiming to probe SHE with muons.

We gratefully acknowledge J. Baas, H. Bonder, M. de Roosz and J. G. Holstein for technical support and funding via the Foundation for Fundamental Research on Matter (FOM), the Netherlands Organisation for Scientific Research (NWO), the Future and Emerging Technologies (FET) programme within the Seventh Framework Programme for Research of the European Commission under FET-Open Grant No. 618083 (CN-TQC), Marie Curie ITN Spinicur NanoLab NL. Part of this work is based on experiments performed at the Swiss muon source SμS, Paul Scherrer Institute, Villigen, Switzerland.

[1]N. Vlietstra, J. Shan, B. J. van Wees, M. Isasa, F. Casanova, and J. Ben Youssef, Phys. Rev. B **90**, 174436 (2014).
[2]G. E. W. Bauer, E. Saitoh, and B. J. van Wees, Nat. Mater. **11**, 391 (2012).
[3]Y. K. Kato, R. C. Myers, A. C. Gossard, and D. D. Awschalom, Science **306**, 1910 (2004).
[4]J. Wunderlich, B. Kaestner, J. Sinova, and T. Jungwirth, Phys. Rev. Lett. **94**, 047204 (2005).
[5]J. Sinova, S. O. Valenzuela, J. Wunderlich, C. H. Back, and T. Jungwirth, Rev. Mod. Phys. **87**, 1213 (2015).
[6]N. Vlietstra, J. Shan, V. Castel, B. J. van Wees, and J. Ben Youssef, Phys. Rev. B **87**, 184421 (2013).
[7]J. E. Sonier, J. H. Brewer, and R. F. Kiefl, Rev. Mod. Phys. **72**, 769 (2000).
[8]R. F. Kiefl, M. D. Hossain, B. M. Wojek, S. R. Dunsiger, G. D. Morris, T. Prokscha, Z. Salman, J. Baglo, D. A. Bonn, R. Liang, W. N. Hardy, A. Suter, and E. Morenzoni, Phys. Rev. B **81**, 180502 (2010).
[9]P. Dalmas de Réotier, A. Maisuradze, A. Yaouanc, B. Roessli, A. Amato, D. Andreica, and G. Lapertot, Phys. Rev. B **93**, 144419 (2016).
[10]Z. Guguchia, H. Keller, R. K. Kremer, J. Köhler, H. Luetkens, T. Goko, A. Amato, and A. Bussmann-Holder, Phys. Rev. B **90**, 064413 (2014).
[11]Z. Salman, T. Prokscha, A. Amato, E. Morenzoni, R. Scheuermann, K. Sedlak, and A. Suter, Phys. Rev. Lett. **113**, 156801 (2014).
[12]E. Morenzoni, R. Khasanov, H. Luetkens, T. Prokscha, A. Suter, N. Garifianov, H. Glückler, M. Birke, E. Forgan, H. Keller, J. Litterst, C. Niedermayer, and G. Nieuwenhuys, Physica B **326**, 196 (2003).
[13]T. Prokscha, E. Morenzoni, K. Deiters, F. Foroughi, D. George, R. Kobler, A. Suter, and V. Vrankovic, Nucl. Instrum. Methods Phys. Res., Sect. A **595**, 317 (2008).
[14]A. Suter, E. Morenzoni, R. Khasanov, H. Luetkens, T. Prokscha, and N. Garifianov, Phys. Rev. Lett. **92**, 087001 (2004).
[15]A. J. Drew, S. L. Lee, D. Charalambous, A. Potenza, C. Marrows, H. Luetkens, A. Suter, T. Prokscha, R. Khasanov, E. Morenzoni, D. Ucko, and E. M. Forgan, Phys. Rev. Lett. **95**, 197201 (2005).
[16]T. Prokscha, E. Morenzoni, K. Deiters, F. Foroughi, D. George, R. Kobler, A. Suter, and V. Vrankovic, Physica B **374–375**, 460 (2006).
[17]P. Bakule and E. Morenzoni, Contemp. Phys. **45**, 203 (2004).
[18]O. Mosendz, V. Vlaminck, J. E. Pearson, F. Y. Fradin, G. E. W. Bauer, S. D. Bader, and A. Hoffmann, Phys. Rev. B **82**, 214403 (2010).
[19]E. Morenzoni, H. Glückler, T. Prokscha, R. Khasanov, H. Luetkens, M. Birke, E. Forgan, C. Niedermayer, and M. Pleines, Nucl. Instrum. Methods Phys. Res., Sect. B **192**, 254 (2002).
[20]H. Nakayama, M. Althammer, Y.-T. Chen, K. Uchida, Y. Kajiwara, D. Kikuchi, T. Ohtani, S. Geprägs, M. Opel, S. Takahashi, R. Gross, G. E. W. Bauer, S. T. B. Goennenwein, and E. Saitoh, Phys. Rev. Lett. **110**, 206601 (2013).
[21]I. A. Merkulov, A. L. Efros, and M. Rosen, Phys. Rev. B **65**, 205309 (2002).
[22]R. I. Dzhioev, V. L. Korenev, I. A. Merkulov, B. P. Zakharchenya, D. Gammon, A. L. Efros, and D. S. Katzer, Phys. Rev. Lett. **88**, 256801 (2002).
[23]J. Strand, B. D. Schultz, A. F. Isakovic, C. J. Palmstrøm, and P. A. Crowell, Phys. Rev. Lett. **91**, 036602 (2003).
[24]V. L. Korenev, Semicond. Sci. Technol. **23**, 114012 (2008).
[25]A. Aqeel, I. J. Vera-Marun, B. J. van Wees, and T. T. M. Palstra, J. Appl. Phys. **116**, 153705 (2014).
[26]S. P. Dash, S. Sharma, J. C. Le Breton, J. Peiro, H. Jaffrès, J.-M. George, A. Lemaître, and R. Jansen, Phys. Rev. B **84**, 054410 (2011).
[27]K.-i. Uchida, J.-i. Ohe, T. Kikkawa, S. Daimon, D. Hou, Z. Qiu, and E. Saitoh, Phys. Rev. B **92**, 014415 (2015).
[28]S. Demokritov, E. Tsymbal, P. Grünberg, W. Zinn, and I. K. Schuller, Phys. Rev. B **49**, 720 (1994).